AGU PUBLICATIONS

Journal of Advances in Modeling Earth Systems

RESEARCH ARTICLE

10.1002/2017MS000994

Key Points:
- G-packed McICA and revised two-stream approximation are developed based on RRTMG for a more efficient and accurate radiation process
- G-packed McICA employs a reduced random number sampling on a reconstructed and unified radiation package
- Revised two-stream approximation provides reduced errors for no significant increase in computational cost

Correspondence to:
S. Baek,
sh.baek@kiaps.org

Citation:
Baek, S. (2017), A revised radiation package of G-packed McICA and two-stream approximation: Performance evaluation in a global weather forecasting model, *J. Adv. Model. Earth Syst.*, *9*, doi:10.1002/2017MS000994.

Received 30 MAR 2017
Accepted 12 JUN 2017
Accepted article online 19 JUN 2017

A revised radiation package of G-packed McICA and two-stream approximation: Performance evaluation in a global weather forecasting model

Sunghye Baek[1]

[1]Development Division Numerical Model Team, Korea Institute of Atmospheric Prediction Systems, Seoul, South Korea

Abstract For more efficient and accurate computation of radiative flux, improvements have been achieved in two aspects, integration of the radiative transfer equation over space and angle. First, the treatment of the Monte Carlo-independent column approximation (MCICA) is modified focusing on efficiency using a reduced number of random samples ("G-packed") within a reconstructed and unified radiation package. The original McICA takes 20% of CPU time of radiation in the Global/Regional Integrated Model systems (GRIMs). The CPU time consumption of McICA is reduced by 70% without compromising accuracy. Second, parameterizations of shortwave two-stream approximations are revised to reduce errors with respect to the 16-stream discrete ordinate method. Delta-scaled two-stream approximation (TSA) is almost unanimously used in Global Circulation Model (GCM) but contains systematic errors which overestimate forward peak scattering as solar elevation decreases. These errors are alleviated by adjusting the parameterizations of each scattering element—aerosol, liquid, ice and snow cloud particles. Parameterizations are determined with 20,129 atmospheric columns of the GRIMs data and tested with 13,422 independent data columns. The result shows that the root-mean-square error (RMSE) over the all atmospheric layers is decreased by 39% on average without significant increase in computational time. Revised TSA developed and validated with a separate one-dimensional model is mounted on GRIMs for mid-term numerical weather forecasting. Monthly averaged global forecast skill scores are unchanged with revised TSA but the temperature at lower levels of the atmosphere (pressure $\geq$ 700 hPa) is slightly increased ($<$ 0.5 K) with corrected atmospheric absorption.

1. Introduction

Physics of radiative transfer is well understood compared to other processes in atmospheric models. However, solving the radiative transfer equation is not an easy task since it requires integration of radiance over multiple dimensions. Several assumptions and approximations are applied at each dimension to reduce the computational cost, but the efficiency always should be balanced with the accuracy since radiative forcing is one of the main driving forces of atmospheric circulation. G-packed McICA and revised two-stream approximation (TSA) are therefore proposed in this study based on the Rapid Radiative Transfer Model for GCMs (RRTMG) [*Iacono et al*., 2008] code which initially incorporates the Monte Carlo-independent column approximation (McICA) [*Pincus et al*., 2003] and a delta-scaled TSA [*Joseph et al*., 1976; *Zdunkowski et al*., 1980].

McICA is an approximation to the full independent column approximation when computing grid-box mean fluxes (ICA) [*Stephens et al*., 1991]. In the ICA method, a grid-box (GCM column) is divided into N subcolumns and the domain-averaged broadband flux $\langle F \rangle^{ICA}$ of the column can be presented using the notation of *Morcrette et al*. [2008],

$$\langle F \rangle^{ICA} = \frac{1}{N} \sum_{n=1}^{N} \sum_{k=1}^{K} c_k F_{n,k} \tag{1}$$

where K is the number of spectral quadrature points related with a correlated-k distribution (CKD) approach [*Lacis and Onias*, 1991] and c_k is the width of the spectrum corresponding to spectral interval k. In the McICA scheme, the flux is computed for each quadrature point using randomly chosen subcolumn as,

$$\langle F \rangle^{McICA} = \sum_{n=1}^{K} c_k F_{n_k,k} \quad (2)$$

where $F_{n_k,k}$ is the monochromatic radiative flux in spectral subinterval k, with a randomly selected vertical cloud distribution n_k.

McICA effectively reduces the computational time of ICA but it contains conditional random noise on the radiative fluxes in common with all other Monte Carlo-based method. Several studies have shown the effect of random noise produced by McICA on the climate. [*Räisänen et al*., 2005, 2008; *Barker et al*., 2008; *Hill et al*., 2011]. McICA random noise can lead to bias in low-cloud fraction and surface temperature, but all GCM simulations tested in the above works showed statistically insignificant impacts on the result. G-packed MCICA is designed to increase the computational efficiency by reducing the number of sub-columns that are generated and reusing the same subcolumns for a number of different spectral intervals. Therefore, it should be validated how reduced sampling affects the performance of GCM simulations. In this study, G-packed McICA is designed for mid-term (10 day) numerical weather prediction with prescribed SST, where the spatial resolution is relatively high. The effect of coarse random sampling on verification skill score is found to be negligible over all regions and atmospheric levels. One-dimensional radiative transfer test with 6700 data columns also shows that flux variation of G-packed McICA is insignificant compared to McICA. Using the same cloud subcolumn (or random sampling) between shortwave and longwave is another distinct feature of G-packed McICA. *Hill et al*. [2011] reported that the net heating errors of short-wave and longwave McICA can effectively canceled out in opposite direction (warming versus cooling) using the same cloud subcolum. Monthly averaged verification skill scores (anomaly correlation, root-mean-square errors and skill scores) of 10 day forecast are not deteriorated with G-packed McCIA.

The delta-scaled TSA is appropriate to simulate strongly peaked forward-scattering by cloud particles in moderately thick cloud layers. The practical improved flux method (PIFM) [*Zdunkowski et al*., 1980] TSA shows slightly better performance than the delta-Eddington method which was first proposed by *Joseph et al*. [1976] but also includes systematic errors. Various assumption used in TSA can cause the systematic errors. One of the main problems is related to the phase function that TSA adopts. All scattering factors used in current radiative model are supposed to be in the Mie scattering regime and approximated by a Henyey-Greenstein (HG) phase function. However, the HG phase function contains biases which may cause important discrepancies [*Boucher*, 1997; *Barker et al*., 2015]. TSA utilize only the asymmetry parameters of the HG phase function, so neglecting details of the phase function adds systematic errors in reflectance, transmittance and absorption [*Barker et al*., 2015]. Delta scaling of TSA further modifies scattering phase function adding systematic errors. Nevertheless, using the exact phase function rather than the HG phase function will significantly complicate solving the radiative transfer equation with higher orders of Legendre expansions. Thus this work focused on reducing systematic errors of TSA by revising other scattering parameters assuming the HG phase function.

The discrete ordinate method with multistream is the most appropriate solution for scattering but unaffordable due to the computational time in GCM. *Räisänen* [2002] shows a very promising alternative to alleviate systematic errors of TSA. The delta-scaled TSA is revised following *Räisänen* [2002] findings for a more exact solution without a significant increase in computation time.

Two separate issues are treated in each section. Section 2 describes methods used for G-packed McICA and revised TSA. Section 3 revises TSA, which describes the method of parameterization using the GRIMs data. Section 4 presents results of each issue while section 5 and section 6 provide impact of numerical weather forecast and conclusion, respectively.

2. Methods

A new radiation package with G-packed McICA and revised two-stream approximation is mounted and tested on the Global/Regional Integrated Model System (GRIMs) [*Hong et al*., 2013]. GRIMs has been created for use in numerical weather prediction (NWP), seasonal simulations, and climate research projects, from global to regional scales. GRIMs is fully tested as a community model, and is currently used as the reference model of the Korea Institute of Atmospheric Prediction Systems (KIAPS) preparing for the national model of Korea Meteorological Administration (KMA). The main components of the current physics package version

Table 1. Components of the Physics Package (Version 11 October 2016) of GRIMs

Radiation	RRTMG [*Iacono et al.*, 2008]
Microphysics	WSM5 MPS [*Hong et al.*, 2004; *Bae et al.*, 2016]
Deep convection	SAS CPS [*Han and Pan*, 2011; *Lim et al.*, 2014; *Han et al.*, 2016]
Shallow convection	GRIMs SCV [*Hong et al.*, 2013]
Planetary boundary condition	YSU PBL [*Hong et al.*, 2006]
Cloud	Prognostic CLD [*Park et al.*, 2016]
Land	NOAH LSM [*Ek et al.*, 2003; *Koo et al.*, 2017]
Convective gravity wave drag	GWDC [*Chun and Baik*, 1998; *Jeon et al.*, 2010]
Orographic gravity wave drag	GWDO [*Kim and Arakawa*, 1995; *Choi and Hong*, 2015]

(11 October 2016) used in this work are listed in Table 1. Initially the radiation package of GRIMs originated from the RRTMG module of the Weather and Research Forecasting (WRF) model [*Skamarock et al.*, 2005].

2.1. G-Packed McICA

2.1.1. Unified Preprocessing for RRTMG

RRTMG in GRIMs, initially transported from WRF has two separate drivers for shortwave and longwave. Prior to applying G-packed McICA, these drivers are unified since G-packed McICA is designed to share the same cloud configuration between shortwave and longwave. In addition to this reason, they are unified in order to avoid various repetitive preprocessing such as setting surface property, computing effective radius, setting cloud hydrometeor property, and filling arrays for the main module of RRTMG etc. Old and new structure of the radiation package are shown in Figure 1. The unified driver also increases flexibility and extensibility of the preprocessing of RRTMG.

2.1.2. Reduced Subcolumns or Random Number Generations

As described above in the equations (1) and (2), a grid-box (GCM column) is divided into N subcolumns in the McICA scheme. Then every layer of each subcolum is filled with a digitized cloud fraction 0 (cloud-free) or 1 (overcast) according to the distributed random number and cloud overlap assumption. Therefore, if the distributed random numbers are the same for A and B subcolumns, they are effectively the same subcolumn with common cloud state. The McICA version of RRTMG called twice in every radiation time step before the main module of shortwave and longwave RRTMG (Figure 1). The number of subcolumns are equal to the number of spectral quadrature points (g-points), so 112 subcolumns for shortwave and 140 subcolumns for longwave. The CPU time consumption of shortwave and longwave McICA takes about 20% of the total radiation process. It can be effectively reduced by G-packed McICA.

G-packed McICA differs from the above version of McICA in two aspects. First, it is designed for both shortwave and longwave avoiding repetitive computations such as creating seed, applying cloud overlap assumption and filling array. Second, the random numbers are generated only for 28 subcolumns instead of 252 (112 shortwave and 140 longwave). Thus the computational efficiency is increased by calling random number generator function less frequently and by applying cloud overlap assumption only for 28 subcolumns. Once cloud overlap assumption is applied on the distributed random numbers of 28 subcolumns, they are copied to the 112 subcolumns of shortwave and 140 of longwave. Twenty eight is the greatest common divider of 112 and 140, therefore 4 copies of 28 subcolumns of shortwave and 5 copies of longwave have the same digitized cloud state. In RRTMG, total number of g-point is equal to the number of subcolumns and this configuration (actual number of subcolumns) is not changed for G-pakced McICA.

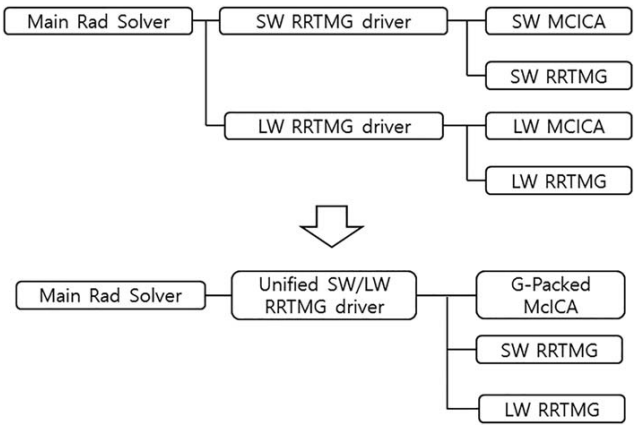

Figure 1. Modified structure of the radiation package in GRIMs with unified shortwave and longwave driver.

The default pseudo random number generator used in this work is specified by *Marsaglia and Zaman* [1993], also known as Keep It Simple Stupid (KISS). KISS shows similar computational performance

with the second option of RRTMG in GRIMs, the Mersenne Twister [*Matsumoto and Nishmura*, 1998] pseudo random number generator. Using faster random number generator will certainly improve the efficiency of McICA. However, different random number generator can make unbiased but different result (see section 4.1.3). We decide to focus on the first impact of G-packed McICA in this study, since all validation tests in KIAPS have been done with *Marsaglia and Zaman* [1993] so far.

Using less random numbers can increase conditional random noise. However, the typical spatial resolution of one grid-box in numerical weather prediction simulation is less than a few tens of kilometers. It is much smaller than the typical grid size of climate simulation and the subcolumn size is sufficient to sample varying cloud status in 10 day forecasts. Test results and the effect of G-packed McICA in terms of accuracy are discussed in section 4.

2.2. Revised Two-Stream Approximation

2.2.1. Modification of Equations

The implicit formulation of the delta two-stream equation for diffuse upward $F^{\uparrow}$, diffuse downward $F^{\downarrow}$ and parallel solar flux S, can be written as follows [*Ritter and Geleyn*, 1992]:

$$\frac{dF^{\uparrow}}{d\tau'}=\alpha_1 F^{\uparrow}-\alpha_2 F^{\downarrow}-\alpha_3\frac{S}{\mu_0}, \tag{3}$$

$$\frac{dF^{\downarrow}}{d\tau'}=\alpha_2 F^{\uparrow}-\alpha_1 F^{\downarrow}+\alpha_4\frac{S}{\mu_0}, \tag{4}$$

$$\frac{dS}{d\tau'}=-\frac{S}{\mu_0}, \tag{5}$$

where μ_0 is the cosine of the solar zenith angle, and τ' is the delta-scaled optical depth. Delta-scaling is parameterized by the forward-peak fraction f [*Joseph et al*., 1976]. In the case of the HG phase function which is commonly used for the Mie scattering regime, $f=g^2$ where g is the asymmetry parameter. Delta-scaled optical properties are as follows:

$$\tau'=(1-\omega f)\tau, \tag{6}$$

$$\omega'=\frac{(1-f)\omega}{1-\omega f}, \tag{7}$$

$$g'=\frac{g-f}{1-f}, \tag{8}$$

where ω is the single-scattering albedo. The coefficients $\alpha_1, \ldots, \alpha_4$ of equations (3)-(5) are defined as

$$\alpha_1=U\{1-\omega'(1-\beta_0)\}, \tag{9}$$

$$\alpha_2=U\beta_0\omega', \tag{10}$$

$$\alpha_3=\omega'\beta(\mu_0), \tag{11}$$

$$\alpha_4=\omega'\{1-\beta(\mu_0)\}, \tag{12}$$

where U is a diffusivity factor, β_0 is the backscattering fraction for diffuse radiation and $\beta(\mu_0)$ is the backscattering fraction for parallel solar radiation. The expression of U, β_0, and $\beta(\mu_0)$ depends on the selected two-stream approximation method. In PIFM, which is the default option of RRTMG in GRIMs,

$$U=2, \tag{13}$$

$$\beta_0=\frac{3}{8}(1-g'), \tag{14}$$

$$\beta(\mu_0)=\frac{1}{4}(2-3g'\mu_0). \tag{15}$$

Traveling through the atmosphere, solar flux is affected by several factors. Most prominently, they are cloud particles in various hydrometeor types, aerosols, gas absorption and Rayleigh scattering which coexist in the atmosphere. In most plane-parallel radiative transfer models with TSA, the layer averaged optical

properties (τ, ω, g) are obtained first then are delta-scaled to compute the coefficietns $\alpha_1, \ldots, \alpha_4$ of equations (3)-(5).

Räisänen [2002] suggested an alternative way to compute $\alpha_1, \ldots, \alpha_4$. Instead of obtaining the layer averaged then delta-scaled optical properties, *Räisänen* [2002] computes delta-scaled optical properties of each factor first then feed these directly into equations (3)-(5) by modifying the summation form over each factor i as follows,

$$\alpha_1 = \frac{1}{\tau'}\left(\sum_i U_i \tau_{a,i} + \sum_i U_i \beta_{0,i} \tau'_{s,i}\right), \tag{16}$$

$$\alpha_2 = \frac{1}{\tau'}\sum_i U_i \beta_{0,i} \tau'_{s,i}, \tag{17}$$

$$\alpha_3 = \frac{1}{\tau'}\sum_i \beta_i(\mu_0) \tau'_{s,i}, \tag{18}$$

$$\alpha_4 = \frac{1}{\tau'}\sum_i (1-\beta_i(\mu_0))\ \tau'_{s,i}. \tag{19}$$

The optical depths are divided by absorption and scattering parts ($\tau' = \tau_a + \tau'_s$) and the absorption optical depth is not affected by delta-scaling. *Räisänen* [2002] separates diffusivity factors for absorption and scattering process, but in this study they are maintained for all factors as 2. Simply transforming equations (9)–(12) to (16)–(19) does not significantly change the results (e.g., see PIFM and PIFM2 of Table 3) [*Räisänen*, 2002]. The advantage of equations (16)–(19) is that we can adjust the optical property of certain layers by selectively changing parameters of each factor. Computation efficiency is also another asset of the method since it requires no significant increase in computing time comparing to multistream method. Modifications of the parameters are done with GRIMs data compared to the results of the multistream discrete ordinate method (DOM). Then validation test is done with independent data set.

2.2.2. Discrete Ordinate Method for Benchmark Solution

The discrete ordinate method (DOM) provides a quasi-exact solution for the radiative transfer equation in a plane-parallel atmosphere. The DISORT algorithm of *Stamnes et al*. [1988] with 16-stream and delta-M scaling [*Wiscombe*, 1977] is connected to RRTMG for the benchmark solution. DISORT is embedded in the spectral loop (g-point) of the SPCVMC_SW subroutine by replacing the TSA solver, REFTRA_SW. The HG phase function is used for all scattering factors. We may get more exact reference result by DISORT using fully accurate phase function, but it is not computationally affordable (or it requires huge size of lookup table) with our model data which contains different effective radius in every layer computed from microphysics. According to *Räisänen* [2002], however, sensitivity tests using *Takeno and Liou* [1989] cirrostratus (Cs) phase function indicated that r.m.s. radiative flux errors that HG phase function caused in 16-delta-DOM (DISORT) calculation were a factor of ~6 smaller than the errors related to the use of delta-Eddington or PIFM approximations for ice clouds. It is unlikely that this simplification affects the results appreciably.

For more efficient test and validation, a one-dimensional radiative transfer module is detached from the RRTMG of GRIMs. The GRIMs data of the independent atmospheric columns are extracted and fed to the one-dimensional radiation model. The radiative transfer equation is solved either by δ-16-DOM (DISORT) or TSA, and the resultant flux is analyzed.

3. Parameterizations With the GRIMs Data

3.1. Data Set

The GRIMs data were obtained from a 10 day forecast run with the current physics package (11 October 2016, Table 1) with initial condition at 12 UTC 25 July 2011. The model uses the National Centers for Environmental Prediction (NCEP) Global Forecast System (GFS) Final (FNL) analysis data and the observed sea surface temperature (SST) and snow data as initial atmospheric and surface boundary conditions. The model has 64 hybrid sigma-pressure vertical levels and a model top pressure of 0.3 hPa and horizontal resolution of T254 (~50 km). The data of 20,129 atmospheric columns are extracted from instantaneous snapshot of 42 and 48 forecast hours which correspond to 06 UTC and 12 UTC. All columns with cosine solar zenith angle $\mu_0 \geq 0.1$ are the selected and number of atmospheric columns at each bin of μ_0 is listed in Table 2.

Table 2. Number of Extracted Atmospheric Columns From the GRIMs Data

μ_0	0.1	0.2	0.3	0.4	0.5	0.6	0.7	0.8	0.9	Total
# of col.	5,250	3,789	1,840	1,633	1,508	1,536	1,525	1,530	1,518	20,129

The extracted atmospheric column data from GRIMs contain solar zenith angle, surface albedo, surface emissivity, surface vegetation type, land mask, layer temperature and pressure, H_2O and O_3 concentration, cloud fraction, cloud water content (liquid, ice and snow), and optical properties of five-type aerosols. The five-type aerosols are black carbon, organic carbon, dust, sea salt and sulfate. Vertical and horizontal distributions of aerosols are obtained from the Monitoring Atmospheric Composition and Climate (MACC) reanalysis. In *Räisänen* [2002], cloud fraction is modified before feeding to DISORT because DISORT cannot handle partial cloudiness, but the cloud fraction of subcolumns are already digitized in McICA, so no modification is required in this study.

In the unified SW/LW RRTMG driver, surface and cloud optical properties are set before calling McICA. The effective radius of the liquid/ice/snow cloud is explicitly computed using the Weather Research forecasting (WRF) single-moment five-class microphysics scheme [*Hong et al*., 2004; *Bae et al*., 2016] with the cloud liquid/ice/snow content of each layer. The range of computed effective radii of cloud particles varies from 5 to 20 μm for liquid, 80 to 200 μm for snow, and 20 to 60 μm for ice. The liquid cloud optical properties are interpolated from the look up table of *Hu and Stamnes* [1993] and the ice cloud optical properties are from *Fu* [1996]. The snow cloud optical properties are not reported in the community yet, so the effective radius is limited to 140 μm and the same look up table of ice cloud is used.

3.2. Modification of TSA Parameterization

The particle's size is the most important factor determining scattering optical properties in the atmosphere. The size of the cloud particle varies depending on the hydrometeor type, cloud water content and temperature thus each optical property differs considerably. The aerosol also has various size, refraction index and shape, which is different from that of cloud particles. *Räisänen* [2002] proposed separate parameterizations for different scattering factors based on this physical reason. The forward-peak scattering fraction *f*, the backscattering fraction for parallel solar radiation $\beta(\mu_0)$, and the backscattering fraction for diffuse radiation β_0 are all tuned for minimizing the statistical errors with respect to δ-16-DOM using the GCM data set. The parameterizations of each scattering factor are determined individually keeping all other factors unchanged. For example, the parameterizations of aerosol $(f, \beta_0, \beta(\mu_0))$ are tuned with default parameterizations (of PIFM) of cloud liquid/ice/snow particles.

The delta-scaled TSA tends to overestimate forward scattering (or underestimate backward scattering) as μ_0 decreases [*Räisänen*, 2002]. This tendency is verified again in this work. All parameterizations are adjusted the suppress the overestimation of forward scattering at low solar elevation. Mainly $\beta(\mu_0)$ is modified knowing the above fact. Other parameters (except aerosol) are not tuned since too many modifications can make hard to interpret the result. Tuning is done by spanning parameter space (increasing *a* of equation (21)) to minimize surface mean error of downward flux, $F^{\downarrow} - F^{\downarrow}_{DISORT}$. There are two reasons why the tuning is done with the mean downward flux error at surface. First, the tuning is mainly done for $\beta(\mu_0)$, which is related to the collimated shortwave beam. The downward flux contains important amount of collimated beam, so the mean error at surface is more effectively and sensitively corrected by tuning $\beta(\mu_0)$. Second, the amount of downward flux is much larger than upward flux in case of shortwave. Tuning the flux at surface boundary is also important for land surface model because the most of fluxes are absorbed 80% in the land 94% in the ocean on average. Of course, the energy balance is equally important in TOA for long-term evolution of GCM. Parameterization may be further refined by tuning β_0 and absorption diffusivity factor in order to reduce the mean in TOA $F^{\uparrow} - F^{\uparrow}_{DISORT}$ error or atmospheric absorption. But the physical basis of tuning these parameters seems weaker than tuning $\beta(\mu_0)$, thus these are not considered in this work. The parameterization of $\beta(\mu_0)$, as a function of μ_0 suggested by *Räisänen* [2002] is replaced by the piecewise linear relation rather than the polynomial fitting curve for the reason of efficiency. The polynomial fitting of each factor requires a higher-ordered exponent or noninteger exponent which substantially increases the computation time.

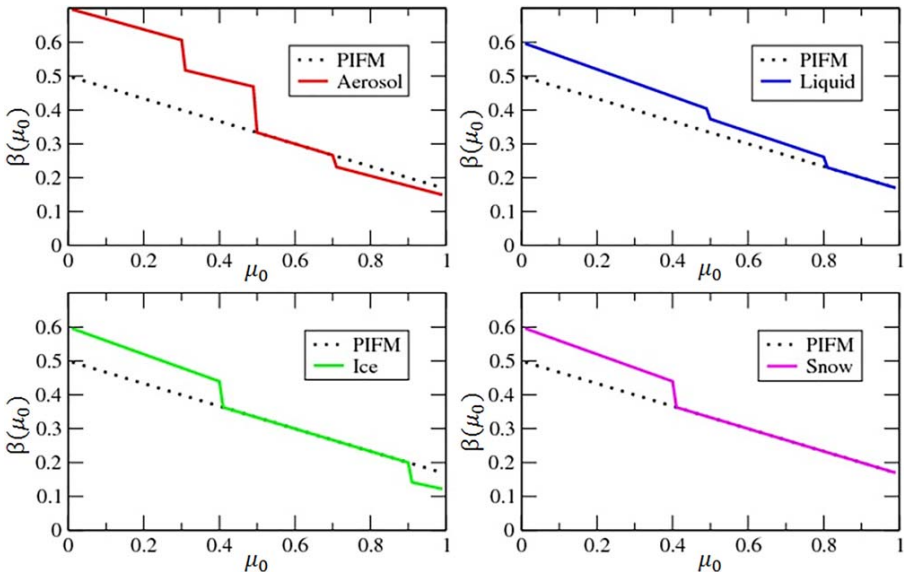

Figure 2. Modification of the backscattering coefficient for parallel solar radiation $\beta(\mu_0)$ as a function of solar zenith angle μ_0 for all scattering factors.

3.2.1. Parameterization of Aerosol

Different from other cloud particles, tuning of all three parameterizations $(f, \beta_0, \beta(\mu_0))$ are necessary for satisfactory results of aerosol. The forward-peak scattering fraction is modified when the cosine of solar zenith angle μ_0 is less than 0.5 to $f=g^{1.5}$, otherwise it is set as the default value, namely $f=g^2$. The backscattering fraction for diffuse radiation β_0 is parameterized as,

$$\beta_0=0.5\times(1-g'), \tag{20}$$

and the backscattering fraction for parallel solar radiation is assumed to be,

$$\beta(\mu_0)=a\ \times(2-3g'\mu_0), \tag{21}$$

where a=0.35 for $0 \le \mu_0 < 0.3$, a = 0.3 for $0.3 \le \mu_0 < 0.5$, a = 0.25 for $0.5 \le \mu_0 < 0.7$, and a = 0.22 for $\mu_0 \ge 0.7$ as shown in Figure 2.

3.2.2. Parameterization of the Cloud Particle

Only the parameterization of $\beta(\mu_0)$ is modified for the cloud particle, as shown in figure. For the liquid cloud particle a = 0.3 for $0 \le \mu_0 < 0.5$, a = 0.28 for $0.5 \le \mu_0 < 0.8$, and a = 0.25 for $\mu_0 \ge 0.8$. For the ice cloud particle a = 0.3 for $0 \le \mu_0 < 0.4$, a = 0.25 for $0.4 \le \mu_0 < 0.9$, and a = 0.18 $\mu_0 \ge 0.9$. For the snow cloud particle, a = 0.3 for $0 \le \mu_0 < 0.4$ and a = 0.25 for $\mu_0 \ge 0.4$.

4. Results

4.1. G-Packed McICA

4.1.1. Efficiency Check

The computational efficiency is the main goal of G-packed McICA. For the 10 day forecast with 64 vertical layer and T254 resolution, McICA CPU consumption is about 20% of the total radiation process. Using G-packed McICA, the CPU consumption is reduced by 70%. Tests made with an Intal(R) Xeon(R) CPU E5–2690 workstation with 64 MPI processors.

4.1.2. Accuracy Check

The 10 day forecasts are run using GRIMs with initial conditions from 1 July 2013 to 31 July 2013 at T254 and 64 vertical resolution. Two experiments are compared, McICA and G-packed McICA. Monthly averaged forecast verification is made with respect to the NCEP GFS FNL analysis data over three global verification areas, northern hemisphere, southern hemisphere and the tropics. The verification scores of geopotential

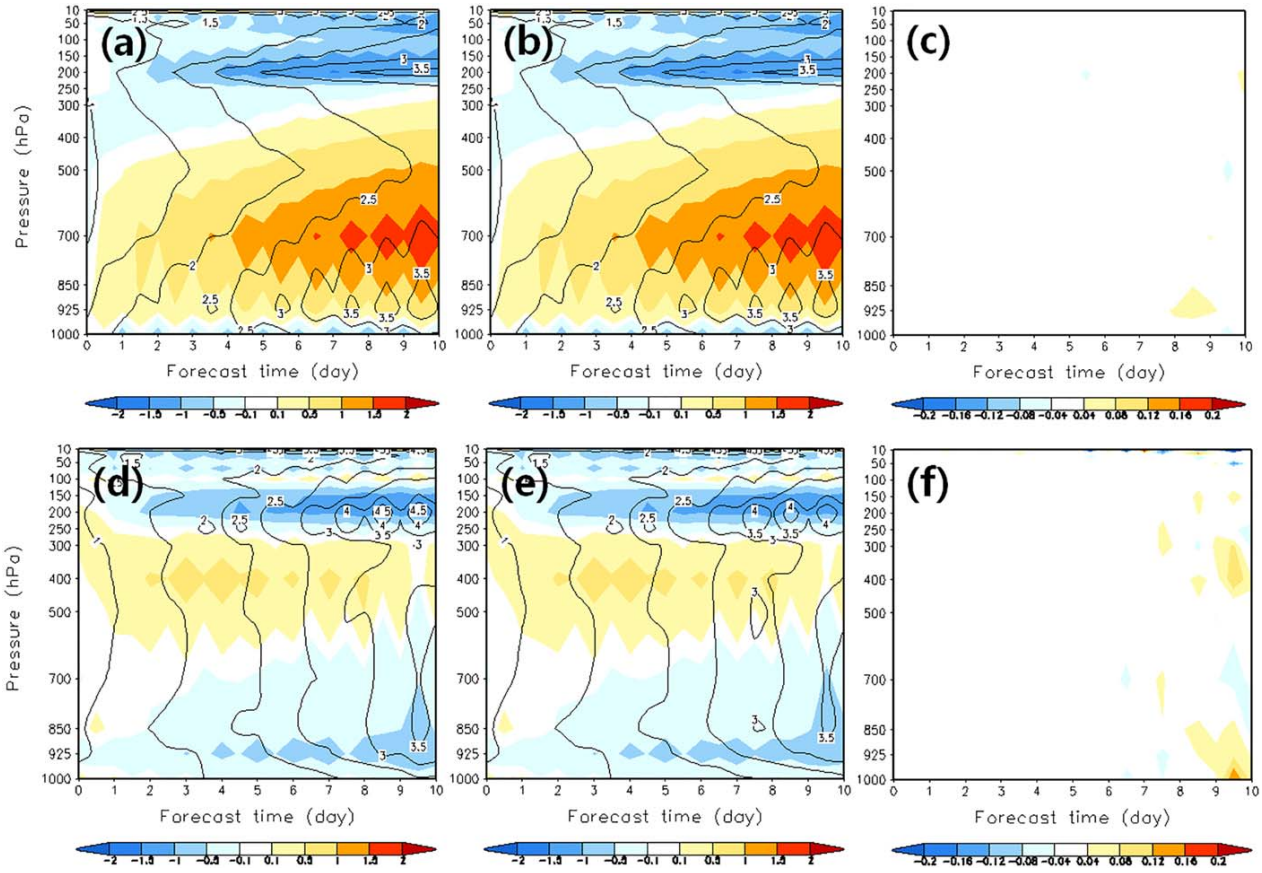

Figure 3. (a) Pressure-time cross sections of averaged bias (shading) and root-mean-square error (contour) of temperature over Asia from McICA, (b) the same graph from G-packed McICA, (c) bias(G-packed McICA)-bias(McICA) over Asia, (d) over Australia from McICA, (e) the same graph from G-packed McICA, (f) bias(G-packed McICA)-bias(McICA) over Australia.

height and temperature (root mean square errors, anomaly correlation and S1 skill scores) in different vertical levels (850, 500, 250, and 100 hPa) show no noticeable difference between McICA and G-packed McICA.

In general, the vertical temperature verification against radiosonde shows more sensitive results than the verification skill scores. Figures 3a, 3b, 3d, and 3e are pressure-time cross sections of monthly averaged bias (shading) and root-mean-square error (contour) of temperature against radiosonde. Figures 3a and 3d are results of McICA, while Figures 3b and 3e are of G-packed McICA. Verifications made in five different regions, Asia, North America, Europe, the Tropics and Australia but only Asia (Figures 3a–3c) and Australia (Figures 3d–3f) are presented since all other regions show very similar feature. The results do not show any noticeable difference either in bias or in contour. The shading colors of Figures 3c and 3f show bias difference of two schemes, *bias*(G-packed McICA)—*bias*(McICA), where the temperature difference is less than 0.1K. The vertical profiles of geopotential height, specific humidity, and wind are also compared with the radiosonde data. The accuracy of G-packed McICA is not deteriorated over all regions. The accuracy is tested by increasing the grid scale up to T62, which provides consistent results.

4.1.3. Impact of Random Number Generator

For a given grid-box (GCM column), G-packed McICA employs less number of random sampling. It is necessary to estimate the noise level of G-packed McICA since poor random sampling can amplify conditional random error. One-dimensional radiation model is used to analyze the result flux of McCIA and G-packed McICA for the same 6700 GRIMs input data. The details of GRIMs input data is as described in section 3.1 except the different initial condition, from 00 UTC 1 February 2014 and extracted instantaneously at 42 forecast hour (18 UTC). Three experiments are done for 6700 data columns, using (1) McICA with *Marsaglia and Zaman* [1993] (KISS), (2) McICA with changed seed, and (3) G-packed McICA with *Marsaglia and Zaman*

Table 3. Mean and Root-Mean-Square-Difference of $F^{\downarrow}_{SW}$, $F^{\downarrow}_{LW}$, $F^{\uparrow}_{SW}$, and $F^{\uparrow}_{LW}$ (W m^{-2}) for Three Experiments: (1) McICA With *Marsaglia and Zaman* [1993] (KISS), (2) McICA With Changed Seed, and (3) G-Packed McICA With *Marsaglia and Zaman* [1993] (KISS)

	Mean of (1)	Mean of (2)	Mean of (3)	RMSD of (1) and (2)	RMSD of (1) and (3)
$F^{\downarrow}_{SW}$ SFC	298.4646	299.8186	298.4553	26.3882	25.33193
$F^{\downarrow}_{LW}$ SFC	342.8767	342.2674	342.9569	5.797856	5.620695
$F^{\uparrow}_{SW}$ TOA	208.2168	207.3187	208.2100	23.68303	22.59423
$F^{\uparrow}_{LW}$ TOA	243.9651	244.1381	243.9114	4.939334	3.817919

[1993] (KISS). The second experiment is performed to estimate the spread due to noise in the original MCICA and the third one is done to estimate the noise level of G-packed McICA. Table 3 shows mean and root-mean-square-difference (RMSD) of downward shortwave ($F^{\downarrow}_{SW}$) and longwave ($F^{\downarrow}_{LW}$) in surface, and upward shortwave ($F^{\uparrow}_{SW}$) and longwave ($F^{\uparrow}_{LW}$) in top-of-atmosphere (TOA) among 6700 data columns. The differences of mean fluxes between G-packed McICA and McICA are very small, less than 0.1 W/m^2 for four all fluxes tested. The differences are slightly smaller than the experiment (2), when the original McICA is run with different seed for random number generator. RMSD of (1)–(2) and (1)–(3) are comparable, the original McIA with different seed shows less spread than G-packed McCIA, but the differences are no greater than 1.1 W/m^2 for all cases. Therefore, we conclude that the flux fluctuation or the noise level of G-packed McICA is comparable to the original McICA with different seed of random number generator.

4.2. Revised Two-Stream Approximation

The atmospheric columns extracted from the GRIMs data are tested with three different radiative transfer solvers: DISORT 16-stream, PIFM TSA and revised TSA with new parameterizations. The GRIMs data used for test are independent from those used for parameterizations. The initial condition starts in boreal winter, 00 UTC 1 February 2014. The 6700 data columns are extracted instantaneously at 42 forecast hour (18 UTC), and 6722 at 48 forecast hour (00 UTC), in total 13,422 columns. Number of atmospheric columns at each bin of μ_0 follows the same ratio as listed in Table 2. Then errors of two TSA methods are obtained comparing to the results of DISORT 16-sream. The percentage of CPU time consumption for the radiation module over a total 10 day forecast of GRIMs is increased from 16% to 17.8% when the revised TSA parameterizations are used.

4.2.1. Mean Error in Surface and Top-Of-Atmosphere

Delta TSA tends to overestimate forward scattering when $\mu_0 \rightarrow 0$. This feature is also observed for PIFM TSA as shown in Figure 4, where the mean error of the downward shortwave difference ($F^{\downarrow}_{PIFM} - F^{\downarrow}_{DISORT}$) increases as μ_0 decreases. Parameterizations are revised to suppress the forward scattering and enhance the backward scattering by modifying the forward-peak scattering fraction and backscattering coefficients. Thus, revised TSA with new parameterizations reduces the mean error of downward shortwave flux at the surface as shown in Figure 4a. Conversely in TOA, the mean error of outgoing shortwave flux of revised TSA shows somewhat degraded performance at the mid solar elevation $0.3 \leq \mu_0 \leq 0.7$. However, we need to consider the error of the entire atmospheric level rather than just the two boundaries (surface and TOA) for complete comparison.

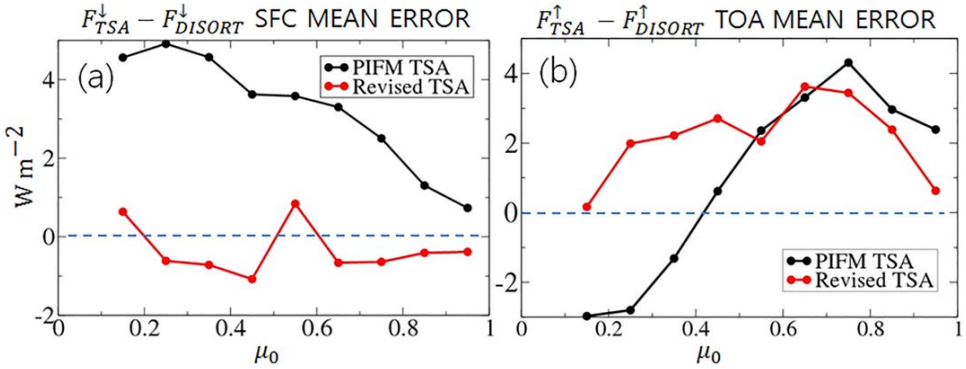

Figure 4. Mean errors of (a) downward shortwave flux at surface and (b) outgoing shortwave flux at top-of-atmosphere.

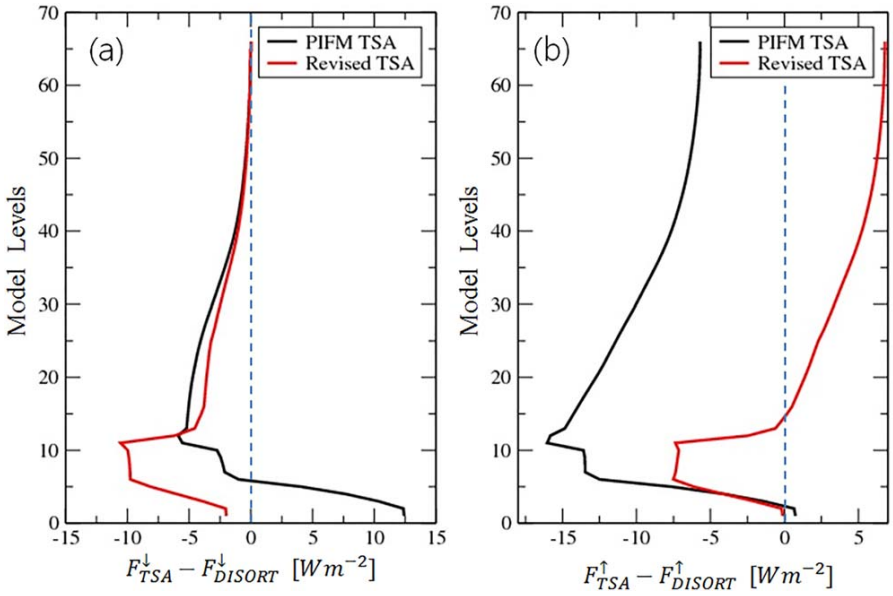

Figure 5. Exemplary flux profiles of one atmospheric column when μ_0=0.49, $\tau_{aerosol}$=0.07, τ_{liquid}=3.56, τ_{ice}=0.03, and τ_{snow}=0. (a) Downward solar flux error and (b) upward solar flux error. RMSE of upward and downward flux at model levels are R_i^{PIFM}=7.30 and $R_i^{Rev.}$=4.53 W m^{-2}, respectively.

4.2.2. Root-Mean-Square Error Over All Atmospheric Layers

An exemplary flux profile of an atmospheric column at mid solar elevation μ_0=0.49 is selected for complete comparison over all atmospheric model levels. The column with mid solar elevation (μ_0=0.49) is chosen because the mean error of revised TSA in TOA is larger than PIFM TSA (Figure 4). The optical depth of the aerosol is $\tau_{aerosol}$=0.07, the liquid cloud τ_{liquid}=3.56, the ice cloud τ_{ice}=0.03 and the snow cloud τ_{snow}=0. Figure 5 shows downward and upward solar flux difference with respect to DISORT over the model levels for the selected atmospheric column. The index of the model starts from the bottom level (lev = 1) to the top level (lev = 64). The results for one column in Figure 5 are consistent with the results of the averaged columns at mid solar elevation. The downward flux of revised TSA at the surface (lev = 1) is close to DISORT but the upward flux of PIFM in TOA (lev = 64) is a little closer to DISORT. However, over all levels, revised TSA is closer to DISORT in both downward and upward solar flux profile. To compare quantitatively the error in all atmospheric levels, we define the root mean square (RMS) of each *i*-column R_i as,

$$R_i = \sqrt{\frac{1}{2N_{lev}}\left[\sum_j^{N_{lev}} \left\{ \left(F^{\downarrow}_{i,j} - F^{\downarrow}_{i,j,DISORT}\right)^2 + \left(F^{\uparrow}_{i,j} - F^{\uparrow}_{i,j,DISORT}\right)^2 \right\}\right]}, \tag{22}$$

where N_{lev} is the level number of model vertical layer where the flux is computed. R_i of the selected column is 7.30 Wm^{-2} for PIFM TSA and 4.53 Wm^{-2} for revised TSA. Thus, revised TSA effectively reduces RMSE by 38% over all the up and down levels, while it has comparable or a bit larger error than PIFM TSA in TOA at the mid solar elevation.

4.2.3. Mean RMS of All Data Columns

For all 13,422 atmospheric columns, the RMS of all the up and down levels, R_i are computed. Mean R_i of each μ_0 bin from 0.1 to 0.9 is presented in the histogram of Figure 6. As discussed in section 3, parameterization of each of the scattering factors are revised to fix errors of TSA which tends to overestimate the forward scattering when the solar zenith angle is large. Figure 6 represents this correction for small μ_0. Overall, revised TSA shows improved performance over PIFM TSA, and errors are effectively corrected for small μ_0. Mean R_i of total columns is reduced by 39%, that is, from 3.66 to 2.26 W m^{-2}.

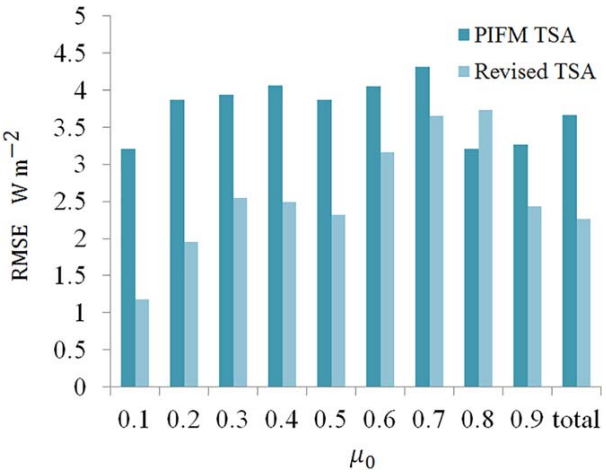

Figure 6. Mean R_i of each μ_0 bin. Mean R_i of all columns is reduced from 3.66 to 2.26 W m^{-2}, by 39%.

4.2.4. Absorption of Revised TSA

One of the advantages of using the formulation (equations (3)–(5)) by *Ritter and Geleyn* [1992] is that we can separate absorption and scattering portions of the coefficients $\alpha_1, \ldots, \alpha_4$ (equations (9)–(12)). Reformulation by *Räisänen* [2002] (equations (16)–(19)) further subdivides the absorption and scattering diffusivity for each factors *i*, so that one can control them individually. According to *Räisänen* [2002], the use of different absorption and scattering diffusivity in idealized test in which each factor was considered alone significantly improved performance, but the advantage proved to be small when all factors were included. For simplicity, all diffusivity factors are fixed ($U=2$) in this study in addition to the above reason.

Even though the diffusivity is not modified in this study, the absorption error is decreased by revising other scattering factors since the solution of radiative the transfer equation (flux at all levels) becomes more close to the quasi-exact solution by DISORT. The average atmospheric shortwave absorption can be defined as,

$$F_{abs} = F_{TOA}^{NET} - F_{SFC}^{NET}, \tag{23}$$

And the mean error according to the cosine of the solar zenith angle μ_0 is shown in Figure 7.

PIFM TSA has negative systematic bias like all other delta-scaled TSA results *Räisänen* [2002] (Table 3). For all solar elevation angles, absorption errors are decreased. The total mean error is reduced from −3.73 to −2.04 W m^{-2} using revised TSA. The slope of downward flux of revised TSA become deeper than PIFM TSA especially under model levels 20, which increases ΔF^{NET} thus absorption.

5. Impacts on Numerical Weather Prediction

Revised TSA developed in the one-dimensional radiative transfer is mounted back to the radiation module of GRIMs. Then using the same initial condition and setting in section 4.1.2, 10 day forecasts are run during July 2013 and compared to NCEP GFS FNL analysis data. No remarkable changes are observed using revised TSA in mid-term (10 day) simulation of NWP, not only for the northern hemisphere, but also the tropics and southern hemisphere. As discussed in section 5.1, revised TSA slightly increases absorption more dominantly in lower pressure levels (700–1000 hPa). This pattern can be found over all regions in vertical temperature comparison against radiosonde. Within 0.5 K difference after 120 forecast hours, bias becomes worse in those areas where there already exists warm bias (East Asia and North America), but improved where there exists cold bias (Europe, the tropics and Australia). Due to the complication of other cloud radiative

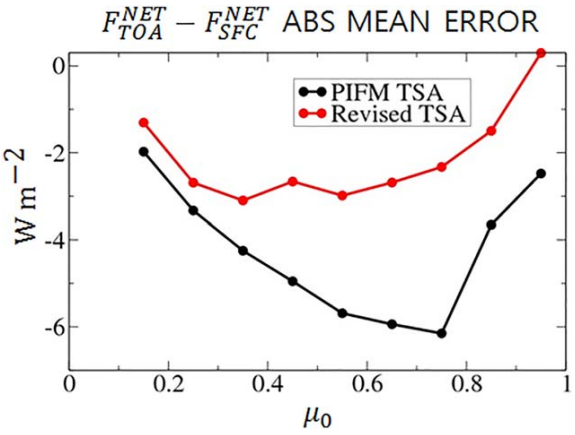

Figure 7. Mean errors of atmospheric absorption of PIFM TSA and revised TSA compare to DISORT.

effect, radiative errors of NWP are more dominant by other sources than use of TSA. However, revised TSA will increase the performance of NWP with other improvement of could scheme, since revised TSA has less systematic errors which other delta TSA contains.

6. Conclusions

G-packed McICA and revised TSA have been developed and tested in GRIMs both focusing on efficiency and accuracy.

The number of random sampling of McICA is reduced by 75% and 80% for shortwave and longwave, respectively. In addition, random numbers are shared between two processes through the unified SW/LW RRTMG driver. The computational time of McICA consumes 20% of the total radiation process, is reduced by 70% using G-packed McICA. The accuracy is also guaranteed in 10 day forecast simulation over all regions. RMSE against NCEP GFS FNL analysis data and vertical radiosonde comparison show that G-packed McICA is accurate enough to be used in NWP. The accuracy is tested by increasing the grid scale up to T62, which provides consistent results. One-dimensional radiative transfer test with 6700 data columns also shows that flux variation of G-packed McICA is insignificant compared to McICA. The flux fluctuation or the noise level of G-packed McICA is comparable to the original McICA with different seed of random number generator. Long-term effects of G-packed McICA on seasonal forecast or climate simulation are not tested in this study, but remains for future work.

The two-stream approximation method is almost unanimously used in GCMs thanks to the efficiency, but delta-scaled TSA contains systematic errors. Delta-scaled TSA overestimates the forward scattering at small μ_0 and underestimate atmospheric absorption over all solar angle. These defects of TSA are corrected by controlling the scattering parameterization of each factor through the reformulation of the radiative transfer equation as proposed in *Räisänen* [2002]. Revised TSA shows significant improvement with respect to 16-stream DOM over all atmospheric levels than PIFM TSA. The mean RMS of all atmospheric columns is reduced by 39%, and the most prominent improvement is found when the cosine of solar zenith angle μ_0 is small. Diffusivity factors are not modified for simplicity, but atmospheric absorption is also improved. The effect of revised TSA on 10 day forecast is not significant in the global averaged verification scores, but shows a minor increase of temperature within 0.5 K after 120 forecast hours in lower model levels caused by increased absorption. Since radiative errors are more dominantly affected by the cloud radiative effect, we cannot expect a significant improvement of NWP performance by revised TSA per se. However, revised TSA reduces systematic errors of the current radiative scheme, underestimation of atmospheric shortwave absorption and overestimation of shortwave at the surface. These errors are found in most present radiative models both compared to observation [*Wild*, 2008] and to line-by-line model [*Pincus et al*., 2015]. The efficiency of revised TSA is also checked through profiling of 10 day forecast of T254. The percentage of CPU time consumption for the radiation module over a total 10 day forecast of GRIMs is increased from 16% to 17.8%. Revised TSA reduces the systematic error of TSA with no significant increase of computational time.

Acknowledgments
This work has been carried out through the R&D project on the development of global numerical weather prediction systems of the Korea Institute of Atmospheric Prediction Systems (KIAPS) funded by the Korea Meteorological Administration (KMA). The author thanks P. Räisänen for helpful advices to embed the DISORT module into the 1-D radiation code and providing the necessary code. Both the data and input files necessary to reproduce the experiments are available via https://www.kiaps.org/eng/business/paper.do. The data are archived at the computing system of KIAPS.

References

Bae, S.-Y., S.-Y. Hong, and K.-S. Lim (2016), Coupling WRF Double-Moment 6-Class Microphysics schemes to RRTMG radiation scheme in weather research forecasting model, *Adv. Meteorol.*, *2016*, 11.

Barker, H. W., J. N. S. Cole, J.-J. Morcrette, R. Pincus, P. Raisanen, K. von Salzen, and P. A. Vaillancourt (2008), The Monte Carlo independent column approximation: An assessment using several global atmospheric models, *Q. J. R. Meteorol. Soc.*, *134*, 1463–1478.

Barker, H. W., J. N. S. Cole, J. Li, B. Yi, and P. Yang (2015), Estimation of errors in two-stream approximations of the solar radiative transfer equation for cloud-sky conditions, *J. Atmos. Sci.*, *72*, 4053–4074.

Boucher, O. (1997), On aerosol direct shortwave forcing and the Henyey-Greenstein phase function, *J. Atoms. Sci.*, *55*, 128–134.

Choi, H.-J., and S.-Y. Hong (2015), An updated subgrid orographic parameterization for global atmospheric forecast models, *J. Geophys. Res. Atmos.*, *120*, 12,445–12,457, doi:10.1002/2015JD024230.

Chun, H.-Y., and J.-J. Baik (1998), Momentum flux by thermally induced internal gravity waves and its approximation for large-scale models, *J. Atmos. Sci.*, *55*, 3299–3310.

Ek, M. B., K. E. Mitchell, Y. Lin, E. Rogers, P. Grunmann, V. Koren, G. Gauno, and J. D. Tarpley (2003), Implementation of Noah land surface model advances in the National Centers for Environmental Prediction operational mesoscale Etamodel, *J. Geophys. Res.*, *108*(D2), 8851, doi:10.1029/2002JD003296.

Fu, Q. (1996), An accurate parameterization of the solar radiative properties of cirrus clouds for climate models, *J. Clim.*, *9*, 2058–2082.

Han, J., and H.-L. Pan (2011), Revision of convection and vertical diffusion schemes in the NCEP Global Forecast System, *Weather Forecast.*, *26*, 520–533.

Han, J.-Y., S.-Y. Hong, K.-S. S. Lim, and J. Han (2016), Sensitivity of a cumulus parameterization scheme to precipitation production representation and its impact on a heavy rain event over Korea, *Mon. Weather Rev.*, *144*, 2125–2135.

Hill, P. G., J. Manners, and J. C. Petch (2011), Reducing noise associated with the Monte Carlo Independent Column Approximation for weather forecasting models, *Q. J. R. Meteorol. Soc.*, *137*, 219–228.

Hong, S.-Y., J. Dudhia, and S.-H. Chen (2004), A revised approach to ice microphysical processes for the bulk parameterization of clouds and precipitation, *Mon. Weather Rev.*, *132*, 103–120.

Hong, S.-Y., Y. Noh, and J. Dudhia (2006), A new vertical diffusion package with an explicit treatment of entrainment processes, *Mon. Weather Rev.*, *134*, 2318–2341.

Hong, S.-Y., et al. (2013), The Global/Regional Integrated Model System (GRIMs), *Asia-Pac. J. Atmos. Sci.*, *49*, 219–243, doi:10.1007/s13143-013-0023-0.

Hu, Y. X., and K. Stamnes (1993), An accurate parametrization of the radiative properties of water clouds suitable for use in climate models, *J. Clim.*, *6*(4), 728–742.

Iacono, M.-J., J. S. Delamere, E. J. Mlawer, M. W. Shepherd, S. A. Clough, and W. D. Collins (2008), Radiative forcing by longlived greenhouse gases: Calculation with the AER radiative transfer models, *J. Geophys. Res.*, *113*, D13103, doi:10.1029/2008JD009944.

Jeon, J.-H., S.-Y. Hong, H.-Y. Chun, and I.-S. Song (2010), Test of a convectively forced gravity wave drag parameterization in a general circulation model, *Asia-Pac. J. Atmos. Sci.*, *46*, 1–10.

Joseph, J. H., W. J. Wiscombe, and J. A. Weinman (1976), The delta-Eddington approximation for radiative transfer, *J. Atmos. Sci.*, *33*, 2452–2459.

Kim, Y.-J., and A. Arakawa (1995), Improvement of orographic gravity wave parameterization using a mesoscale gravity wave model, *J. Atmos. Sci.*, *52*, 1875–1902.

Koo, M.-S., S. Baek, K.-H. Seol, and K. Cho (2017), Advances in land surface modeling of KIAPS based on the Noah land surface model, *Asia-Pac. J. Atmos. Sci.*, doi:10.1007/s13143-017-0043-2, in press.

Lacis, A., and V. Onias (1991), A description of the correlated-k distribution method for modeling nongray gaseous absorption, thermal emission, and multiple scattering in vertically inhomogeneous atmospheres, *J. Geophys. Res.*, *96*, 9027–9064.

Lim, K.-S., S.-Y. Hong, J.-H. Yoon, and J. Han (2014), Simulation of the summer monsoon rainfall over East Asia using the NCEPGFS cumulus parameterization at different horizontal resolutions, *Weather Forecast.*, *29*, 1143–1154.

Marsaglia, G., and A. Zaman (1993), The KISS generator, technical report, Dep. of Stat., Fla. State Univ., Tallahassee.

Matsumoto, M., and T. Nishmura (1998), Mersenne Twister: A 623-dimensionally equidistributed uniform pseudorandom number generator, *ACM Trans. Model. Comput. Simul.*, *8*, 3–30.

Morcrette, J.-J., H. W. Barker, J. N. S. Cole, M. J. Iacono, and R. Pincus (2008), Impact of a new radiation package, McRad, in the ECMWF integrated forecasting system, *Mon. Weather Rev.*, *136*, 4773–4798.

Park, R.-S., J.-H. Chae, and S.-Y. Hong (2016), A revised prognostic cloud fraction scheme in a global forecasting system, *Mon. Weather Rev.*, *114*, 1219–1229.

Pincus, R., H. W. Barker, and J.-J. Morcrette (2003), A fast, flexible, approximate technique for computing radiative transfer in inhomogeneous cloud fields, *J. Geophys. Res.*, *108*(D13), 4376, doi:10.1029/2002JD003322.

Pincus, R., et al. (2015), Radiative flux and forcing parameterization error in aerosol-free clear skies, *Geophys. Res. Lett.*, *42*, 5485–5492, doi:10.1002/2015GL064291.

Räisänen, P. (2002), Two-stream approximations revisited: A new improvement and test with GCM data, *Q. J. R. Meteorol. Soc.*, *128*, 2397–2416.

Räisänen, P., H. W. Barker, and J. N. S. Cole (2005), The Monte Carlo independent column approximation's conditional random noise: Impact on simulated climate, *J. Clim.*, *18*, 4715–4730.

Räisänen, P., S. Järvenoja, and H. Järvinen (2008), Noise due to the Monte Carlo independent-column approximation: Short-term and long-term impacts in ECHAM5, *Q. J. R. Meteorol. Soc.*, *134*, 481–495.

Ritter, B., and J.-F. Geleyn (1992), A comprehensive radiation scheme for numerical weather prediction models with potential applications in climate simulations, *Mon. Weather Rev.*, *120*, 303–325.

Skamarock, W. C., J. B. Klemp, J. Dudhia, D. O. Gill, D. M. Barker, W. Wang, and J. G. Powers (2005), A description of the advanced research WRF version2, *NCAR Tech. Note NCAR/TN-468+STR*, 88 pp., NCAR.

Stamnes, K., S.-C. Tsay, W. Wiscombe, and K. Jayaweera (1988), Numerically stable algorithm for discrete-ordinate-method radiative transfer in multiple scattering and emitting layered media, *Appl. Optics*, *27*, 2502–2509.

Stephens, G. L., P. M. Gabriel, and S.-C. Tsay (1991), Statistical radiative transfer in one-dimensional media and its application to the terrestrial atmosphere, *Trans. Theory Stat. Phys.*, *20*, 139–175.

Takeno, Y., and K.-N. Liou (1989), Solar radiative transfer in cirrus clouds. Part I: Single-scattering and optical properties of hexagonal ice crystals. *J. Atmos. Sci.*, *46*, 3–19.

Wild, M. (2008), Short-wave and long-wave surface radiation budgets in GCMs: A review based on the IPCC-AR4/CMIP3 models, *Tellus, Ser. A*, *60*, 932–945.

Wiscombe, W. J. (1977), The delta-M method: Rapid yet accurate radiative flux calculations for strongly asymmetric phase functions, *J. Atmos. Sci.*, *34*, 1408–1422.

Zdunkowski, W. G., R. M. Welch, and G. Korb (1980), An investigation of the structure of typical two-stream methods for the calculation of solar fluxes and heating rates in clouds, *Beitr. Phys. Atmos.*, *53*, 147–166.